REPORT DOCUMENTATION PAGE

Form Approved
OMB No. 0704-0188

1. REPORT DATE *(DD-MM-YYYY)*	2. REPORT TYPE	3. DATES COVERED *(From - To)*
8 May 2003	Technical Paper	

4. TITLE AND SUBTITLE

High Thrust to Weight Bipropellant Reentry Vehicle Thrust Vector Control Thru Micro-Miniaturization

5a. CONTRACT NUMBER

5b. GRANT NUMBER

5c. PROGRAM ELEMENT NUMBER

6. AUTHOR(S)

William Figueiredo

5d. PROJECT NUMBER
4847

5e. TASK NUMBER
0255

5f. WORK UNIT NUMBER

7. PERFORMING ORGANIZATION NAME(S) AND ADDRESS(ES)

Air Force Research Laboratory (AFMC)
AFRL/PRST
4 Draco Drive
Edwards AFB CA 93524-7160

8. PERFORMING ORGANIZATION REPORT NUMBER

AFRL-PR-ED-TP-2003-131

9. SPONSORING / MONITORING AGENCY NAME(S) AND ADDRESS(ES)

Air Force Research Laboratory (AFMC)
AFRL/PRS
5 Pollux Drive
Edwards AFB CA 93524-7048

10. SPONSOR/MONITOR'S ACRONYM(S)

11. SPONSOR/MONITOR'S NUMBER(S)
AFRL-PR-ED-TP-2003-131

12. DISTRIBUTION / AVAILABILITY STATEMENT

Approved for public release; distribution unlimited.

13. SUPPLEMENTARY NOTES

14. ABSTRACT

15. SUBJECT TERMS

16. SECURITY CLASSIFICATION OF:			17. LIMITATION OF ABSTRACT	18. NUMBER OF PAGES	19a. NAME OF RESPONSIBLE PERSON
					Sheila Benner
a. REPORT	b. ABSTRACT	c. THIS PAGE	A		19b. TELEPHONE NUMBER *(include area code)*
Unclassified	Unclassified	Unclassified			(661) 275-5693

FILE

MEMORANDUM FOR PRS (In-House Publication)

8 May 2003

FROM: PROI (STINFO)

SUBJECT: Authorization for Release of Technical Information, Control Number: **AFRL-PR-ED-TP-2003-131**
William Figueiredo (AFRL/PRST), "High Thrust to Weight Bipropellant Reentry Vehicle Thrust Vector Control Thru Micro-Miniaturization"

5361

(Statement A)

AIAA Joint Propulsion Conference
(Huntsville, AL, 20-23 July 2003) (Deadline = 13 May 2003)

HIGH THRUST TO WEIGHT BIPROPELLANT REENTRY VEHICLE THRUST VECTOR CONTROL THRU MICRO-MINIATURIZATION

William A. Figueiredo*
Air Force Research Laboratory
Propulsion Directorate
Edwards AFB, California

Abstract

With the advent of nanosat and picosat-size satellites, the design of miniature, efficient, high thrust-to-weight (T/W) ratio thrust vector control (TVC) thrusters with liquid bipropellants has been evolving. The extremely high T/W ratios achievable with micro miniaturization of liquid bipropellant engines are a result of the "cube-square-law". As the engine is scaled down linearly, the propellant flow, and thus the power, decreases with chamber cross-sectional area or the square of the linear size, while the weight decreases with the volume of the engine or the cube of the linear size. As a result, the power-to-weight ratio increases linearly as the engine size is reduced. Only recently, by going to micron-scale microelectromechanical system (MEMS) silicon wafer fabrication technology, has the increase in T/W ratio at reduced bipropellant engine scales been realized over existing T/W ratios for TVC thrusters. MEMS and possibly nanotechnology fabrication techniques are the enabling technologies for achieving these higher propulsive system T/W ratios. A fundamental problem with achieving high specific impulse or thrust performance at these reduced engine scales is the combustion residence time. By increasing combustion chamber pressure and adjusting oxidizer to fuel mixture ratio to fuel rich at these reduced engine scales, efficient bipropellant combustion is shown to be analytically and experimentally achievable at engine characteristic lengths one to two orders of magnitude smaller then characteristic lengths of typical spacecraft or satellite TVC thrusters. The advantages of using reduced scale TVC thrusters in improving reentry vehicle (RV) targeting accuracy and mission impulse requirements will be discussed with RV and nano RV reaction control systems.

I. Introduction

The extremely high T/W ratios achievable with micro-miniaturization of liquid bipropellant engines are a result of the "cube-square-law."[1] As the engine is scaled down linearly, the propellant flow, and thus the power, decreases with chamber cross-sectional area (the square of the linear size) while the weight decreases with volume of the engine (the cube of the linear size) so that the power-to-weight or T/W ratio increases linearly as the engine size is reduced. Two different fabrication technologies are investigated in pursuing this high T/W goal. The first is MEMS silicon wafer technology being applied to micro propulsion research by the Massachusetts Institute of Technology (MIT). The second approach[2], developed by the Air Force Research Laboratory (AFRL), involves micro-machining conical nozzle geometries with circular throats down to approximately 50μm. The AFRL fabrication approach is applicable to high-temperature rare-earth materials typically used in radiation-cooled TVC nozzles such as rhenium, or tungsten. The primary advantage of the AFRL micro-nozzle fabrication approach is the capability of surviving the corrosive environments of storable hypergolic propellants, such as hydrazine, used in satellite TVC or deep-space propulsion applications. A proof of principle micro-nozzle of nickel fabrication with the AFRL approach is shown in Figure 1.

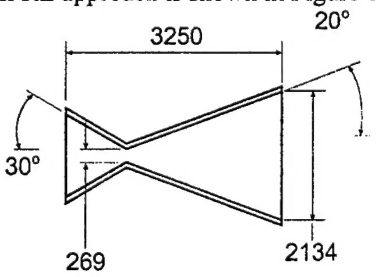

Figure-1. AFRL Micronozzle Schematic. All Dimensions in μm. (Ketsdever, 1999)

The MIT MEMS fabrication approach results in a high aspect ratio rectangular bipropellant engine assembled from silicon wafers. MIT has developed MEMS fabrication procedures for turbo-pumps, regenerative-cooled rocket combustion chambers and nozzles, propellant injectors, and has also experimentally

*Member AIAA, Aerospace engineer

demonstrated these components[3,4]. The general arrangement of the MIT engine is shown in Figure 2.

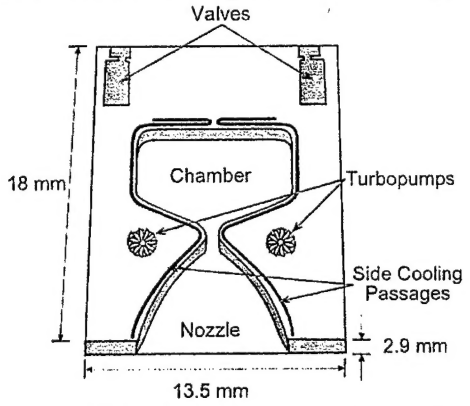

Figure-2. MIT MEMS Bipropellant Engine General Arrangement (London,2000)

By modeling the combustion chamber and nozzle as a pressure vessel[5], the process of achieving high T/W ratio can be understood. The following pressure vessel equation describes how the thrust chamber T/W ratio increases with reduction in scale.

$$\frac{F}{m} \propto \frac{P_c A_T C_f}{P_S SAL} \propto \frac{L^2 C_f}{L^3} = \frac{C_f}{L^*} \propto \frac{1}{L^*} \qquad (1)$$

Once the chamber pressure reaches a certain level, and if the exit nozzle has a large exit to throat area ratio, then the thrust coefficient really is not changing dramatically, so the principle mechanism for chambers T/W increase is reduction in chamber characteristic length. Historical engine weight trends do not support this miniaturization hypothesis when engine chamber T/W ratio is plotted versus engine chamber weight as shown in Figure 3.

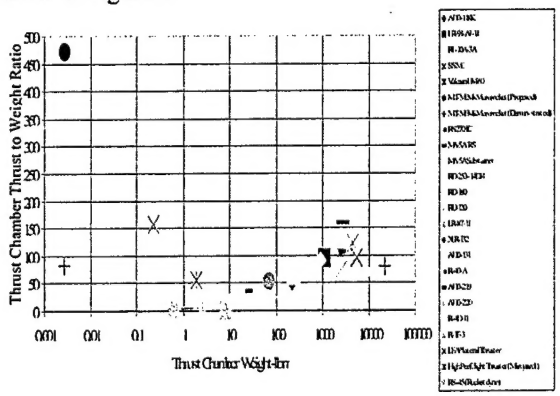

Figure-3. Bipropellant Thrust Chamber T/W Ratio versus Chamber Weight

Figure 3 indicates that for smaller and smaller thrust chamber weights, the lower the chamber T/W ratio. Except for the MIT MEMS engine and the Marquardt LEAP thruster, this trend seems counter-intuitive to the analytical argument put forth in Equation 1. The reason for this trend reversal can be explained by plotting chamber T/W ratio versus the Bayt characteristic length parameter[5], C_f/L^*, as shown in Figure 4.

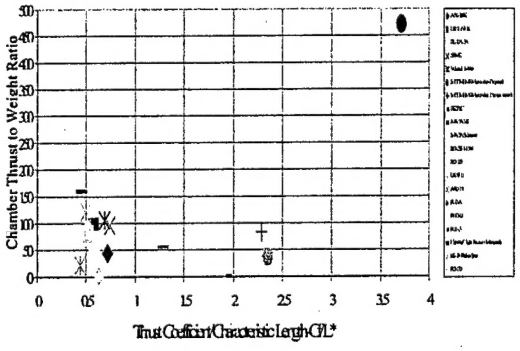

Figure-4. Bipropellant Thrust Chamber T/W Ratio versus C_f/L^*

Figure 4 indicates that very few rocket engines have really small characteristic lengths representative of the MIT MEMS rocket engine $(L^* \sim .25 feet)$. Most bipropellant engines have a C_f/L^* of approximately 0.55 with a characteristic length around 3 to 4 feet. In order to achieve truly high T/W ratios, bipropellant engines of very short characteristic length have to be developed to take advantage of the pressure vessel scaling equation (Eq. 1). Either the MIT MEMS or the AFRL metal micro-nozzle fabrication approach achieve the high T/W ratios predicted by Equation 1. MIT has experimentally proven that bipropellant rocket T/W ratio increases at reduced engine characteristic length (Figure 3) but not as high as originally proposed[3] (T/W equal to 1200). MIT would have experimentally demonstrated a much higher T/W ratio by going to thinner gauge silicon wafer material then used on their prototype engine which was designed to operate at 125 atm. The experimental tests, only achieved a combustion chamber pressure of 12 atm.

To take advantage of the enhanced T/W ratio at reduced engine scales, several issues that diminish performance at reduced engine scales have to be addressed. The first issue is the reduced chamber

residence time at reduced engine scales requiring shorter and shorter liquid bipropellant combustion residence times. The chamber residence time is given by the following equation[6]

$$\tau_{res} = \frac{\rho_c V_c}{\dot{m}} \tag{2}$$

Reference 6 further notes that $\rho_c / \dot{m}$ is independent of chamber pressure such that chamber residence time is independent of chamber pressure, but combustion residence time is not. By increasing the chamber combustion pressure, and adjusting the oxidizer to fuel ratio to fuel rich as described in the theoretical section, the combustion residence time can be shortened to the desired values below the chamber residence time.

Another important factor at reduced engine length scales, is the high heat loss in relation to heat generated during combustion[7]. The heat loss in relation to heat generated is inversely proportional to the engine characteristic length according to the following relationship.

$$\frac{E''}{\dot{E}} \propto \frac{1}{d_h^{1.2}} \tag{3}$$

where E'' is the heat loss in relation to the heat generated, $\dot{E}$. At the high power to weight ratios associated with the small engine characteristic lengths utilizing MEMS fabrication techniques, regenerative cooling would be required to recover the high heat losses during combustion[1]. Therefore, with regenerative cooling, high specific impulse operation can be achieved with very small engine characteristic lengths, lengths on the order of 0.1 to 1 inch.

The next performance reducing phenomena at reduced length scales is the aerodynamic losses associated with small scale rocket vehicles[8]. To understand the effect of scale upon the effective specific impulse, the rocket delta-V equation is used with losses[8] ,or

$$\Delta V = \Delta V_{delivered} - \Delta V_{gravity} - \Delta V_{drag} - \Delta V_{steering} \tag{4.a}$$

$$\Delta V = g_o I_{sp} In \frac{M_{inital}}{m_{final}} - \int_0^{t_{bo}} g \cos\theta dt - \int_0^{t_{bo}} \frac{C_d A_{ref} \frac{1}{2} \rho_{atm} V^2}{m} dt - \int_0^{T_{bo}} \frac{F}{m}(1 - \cos\alpha_c) dt \tag{4.b}$$

For very small rocket vehicles, the vehicle mass, m, is small in relation to the cross-sectional drag area, $C_d A_{ref}$. This reduction in vehicle ballistic coefficient, $m / C_d A_{ref}$, causes ΔV losses in vehicle performance for very small vehicles. Figure 5 shows the effect of air drag upon launch vehicle performance. As the launch vehicle gross takeoff weight is reduced, the drag loss portion of total ΔV increases, and the payload mass fraction is reduced. Figure 5 indicates that the larger the launch vehicle ballistic coefficient, $m / C_D A_{ref}$, the larger the vehicle payload mass fraction. This implies that in order to take advantage of the high T/W ratio performance enhancement of small scale rocket engines, they should be clustered into larger arrays propelling larger vehicles[1]. In this way, the reduction in propulsive system weight in relation to the overall vehicle weight, would be realized without a corresponding loss in payload mass fraction due to the enhanced effects of air drag.

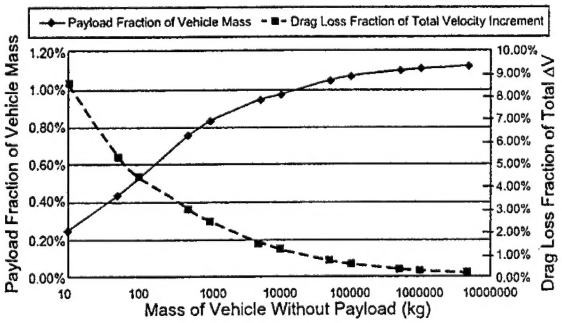

Figure-5. Effects of Air Drag on Launch Vehicle Performance (770 km Orbit/90 deg. Inclination/Ground Launched) (Francis, 1999)

A beneficial implication of the delta-V equation for small vehicles is during atmospheric reentry. While the delta-V equation (Eq. 4.b) states that payload mass fraction of a reduced-scale launch vehicle is significantly reduced, this is not the case for

a reduced-scale weapon payload such as a nano RV. If you eliminate the thrust terms of the delta-V equation (Eq. 4b), and translate the coordinate system from a vertical launch system to a horizontal reentry vehicle coordinate system, the equation reduces to the deceleration equation for a RV, or

$$\frac{-dV}{dt} = -g\sin\theta + \frac{C_d A_{ref}}{m} \cdot \frac{\rho V^2}{2} \qquad (4.c)$$

For a reduced-scale RV, such as a nano RV, the vehicle decelerates more quickly during atmospheric reentry due to the lower ballistic coefficient, $m/C_D A_{ref}$. This results in the nano RV decelerating below plasma shielding speed more quickly allowing the GPS/INS guidance system to acquire targeting coordinates with more time before impact. As a result micro-miniaturization helps you achieve targeting objectives, either thru microthruster TVC enhancing pointing accuracy, or through the enhanced deceleration of reduced-sized RVs. The advantages of using reduced-scale TVC thrusters in improving RV targeting accuracy and mission impulse requirements will be discussed with RV and nano RV reaction control systems.

II. Theoretical Analysis

II.A. Microthruster Combustion Residence Time Analysis

In the interest of finding how small a bipropellant engine can be made and still achieve respectable specific impulse performance, a more detailed analysis of the combustion residence time as a function of chamber pressure and oxidizer to fuel (O/F) ratio was made. The combustion residence time modeling that AFRL did involved data matching more detailed theoretical combustion residence time analysis done by MIT[9]. MIT used two different computational methods described in References 10, 11, and 12. A more detailed discussion of the MIT MEMS bipropellant engine design condition be found in Reference 3 and was for a propellant mixture of ethanol and oxygen at a 125-atm chamber pressure. The MIT combustion residence time analysis results are shown in Figure 6 versus combustion temperature.

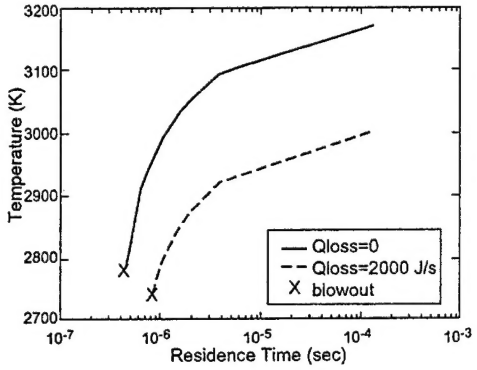

Figure-6. Chemical Kinetics Residence Time for Ethanol and Oxygen (O.M. Al-Midani, 1998)

The interesting result of the MIT analysis is that the shortest combustion residence time occurs at the lowest combustion temperature near the fuel-rich blowout limit. This occurs at a O/F ratio of 1.15 at a combustion temperature of 2700 degrees Kelvin as shown in Figure 7.

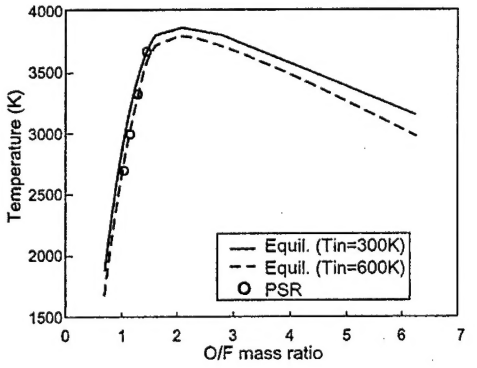

Figure-7. Combustion Chamber Equilibrium Temperatures for Different O/F Ratios for Ethanol and Oxygen (O.M. Al-Midani, 1998)

At the stoichiometric O/F mixture of 2.2, where the highest obtainable combustion temperature occurs, the combustion time is orders of magnitude larger than the fuel-rich cases, and stoichiometric combustion is not considered possible for the short 0.1-msec chamber residence time of the MIT MEMS bipropellant engine. This was eventually proven by MIT experimentally when their MEMS engine only operated over the narrow fuel-rich range shown in Figure 10.

II.B. Bimolecular Chemical Kinetics Combustion Model

From the MIT analysis results in Figure 6, the combustion residence time appears to be proportional to the Arrhenius activation energy, which is reduced at the lower fuel-rich combustion temperatures resulting in reduced combustion residence time. This forms the basis of data matching the MIT combustion analysis[9] with a more general bimolecular chemical kinetics combustion model utilizing Arrhenius activation energy modeling to calculate combustion residence time[13]. The second-order chemical kinetics rate equation is defined as

$$\frac{-dN_A}{dt} = K_{AB} \cdot N_A \cdot N_B \qquad (5.a)$$

where

$$K_{AB} = \frac{\dfrac{-dN_A}{dt}}{N_A \cdot N_B} \qquad (5.b)$$

N_A and N_B are respectively the number of fuel and oxidizer molecules per unit volume, and K_{AB} is the second-order combustion rate constant for unlike fuel and oxidizer molecules. For combustion of fuel and oxidizer molecules at a given O/F ratio, the following stoichiometric equation is used.

$$A + bB = eE + fF \qquad (6)$$

For the above general reaction under steady state, the rate of combustion of fuel to oxidizer molecules is

$$\frac{-dN_A}{dt} = -\frac{1}{b} \cdot \frac{dN_B}{dt} = \frac{dx}{dt} = K_{AB} \cdot N_A \cdot N_B \qquad (7)$$

X is defined as the number of molecules of combustion products created per unit volume. Integration of the above rate equation yields

$$\left(N_{A_o} - N_A\right) = \left(\frac{N_{B_o} - N_B}{b}\right) = x \qquad (8)$$

N_{AO} and N_{BO} are the initial number of fuel and oxidizer molecules per unit volume prior to combustion. By rearranging equation 5.a, 7, and 8, and solving for $\dfrac{dx}{dt}$, we get the following equation for combustion products generated.

$$\frac{dx}{dt} = K_{AB} \cdot b \cdot (N_{A_o} - x)^2 = K_{2B} \cdot \left(N_{A_o} - x\right)^2 \qquad (9)$$

Equation 5.a for unlike molecules, N_A and N_B has been reduced to a kinetics rate equation for like N_A molecules, where K_{2B} is the second-order combustion rate constant for like fuel and oxidizer molecules. The solution to Equation 9 is[14]

$$\frac{x(t)}{N_{A_o}} = \frac{N_{A_o} \cdot b \cdot K_{AB} \cdot t}{(1 + N_{A_o} \cdot b \cdot K_{AB} \cdot t)} \qquad (10)$$

where

$$N_{A_o} \cdot b \cdot K_{AB} = \frac{1}{\tau} \qquad (11)$$

and τ is defined as a combustion time constant. For complete combustion, we assume the ratio of combustion products concentration to the initial fuel concentration is complete at 85 percent or

$$\frac{x(t)}{N_{A_o}} = 0.85 = \frac{t/\tau}{1 + t/\tau} \qquad (12.a)$$

or

$$\tau_{comb} = 6\tau = \frac{6}{N_{A_o} \cdot b \cdot K_{AB}} \qquad (12.b)$$

To calculate the combustion rate constant, K_{AB}, the kinetic theory of gases is used. The number of bimolecular collisions, Z_{AB}, between unlike molecules A and B per unit volume per unit time is given by the following expression

$$Z_{AB} = \pi \cdot {\sigma_{AB}}^2 \cdot \overline{V}_r \cdot N_A \cdot N_B \qquad (13)$$

where the average molecular diameter, σ_{AB}, is

$$\sigma_{AB} = \frac{\sigma_A + \sigma_B}{2} \qquad (14)$$

The mean relative molecular speed, $\overline{V}_r$, of type A and B molecules is

$$\overline{V}_r = \left(\frac{8 \cdot K_b \cdot T_{comb}}{\pi \cdot \mu} \right)^{\frac{1}{2}} \tag{15}$$

and the reduced molecular mass, μ, is

$$\mu = \frac{m_a \cdot m_b}{(m_a + m_b)} \tag{16}$$

The average molecular diameter, σ_{AB}, can be calculated from molecular diameter tables in Reference 15.

Since the number of molecules which react per unit time, is much less than those entering into collision, an Arrhenius activation energy function is derived to calculate the number of reactant molecules that do react. This expression is defined as

$$\frac{Z'}{Z_{AB}} = S \cdot e^{\frac{-E_o}{R_{mix} \cdot T_{comb}}} \tag{17}$$

where Z' is the number of effective bimolecular collisions per unit volume per unit time, and E_O is the activation energy threshold that the colliding molecules have to exceed to achieve reaction. R_{mix} is the universal gas constant of the reactant gas mixture and T_{comb} is the combustion temperature, S is the steric factor, a collision impact orientation factor for the number of molecules that have the proper orientation for reaction. For the purposes of this theoretical investigation where we are just data matching MIT combustion data, S is assumed to be one. The combustion activation energy is chosen to match both the theoretical data shown in Figure 6, and MIT experimental data obtained from Reference 3 and 6. Finally, by combining results from equation 5.b, 13 and 17, we get the following expression for the bimolecular combustion rate constant or

$$K_{AB} = -\frac{-d N_A / dt}{N_A \cdot N_B} = \frac{Z'}{N_A \cdot N_B} \tag{18}$$

$$= \pi \cdot \sigma_{AB}^2 \cdot \overline{V}_r \cdot S \cdot e^{\frac{-E_o}{R_{mix} \cdot T_{comb}}}$$

To calculate the time constant, τ_{comb}, in equation 12.b, and to calculate the mixture gas constant, R_{mix}, the oxidizer stoichiometric coefficient, b, in Equation 6 is calculated with the following equation

$$b = \left(\frac{O}{F} \right) \cdot \left(\frac{M_{fuel}}{M_{oxidizer}} \right) \tag{19}$$

where O/F is the oxidizer to fuel ratio by weight and M_{fuel} and $M_{oxidizer}$ are the molar molecular weight of the fuel and oxidizer. Once the stoichiometric coefficient has been calculated, then the following expressions[16] are used for calculating R_{mix}. The mole fractions, x_i, for the fuel and oxidizer can be shown to be

$$x_a = \frac{1}{1+b} \quad \text{and} \quad x_b = \frac{b}{1+b} \tag{20}$$

$$x_a = \frac{P_a}{P} \quad \text{and} \quad x_b = \frac{P_b}{P} \tag{21}$$

where P is the combustion pressure, and P_a and P_b are the fuel and oxidizer partial pressures. With the partial pressures P_a and P_b from Equation 21, the fuel and oxidizer freestream densities prior to combustion can be determined with the perfect gas law, or

$$\rho_a = \frac{P_A}{R_a \cdot T_{comb}}, \rho_b = \frac{P_B}{R_B \cdot T_{comb}} \tag{22}$$

The fuel and oxidizer gas constants are calculated with

$$R_A = \frac{R}{M_A} \quad \text{and} \quad R_B = \frac{R}{M_B} \tag{23}$$

where R is the universal gas constant and M_A and M_B are the fuel and oxidizer molar weight.
Finally, the gas constant of the combustion gas mixture is calculated with

$$R_{mix} = \frac{\rho_A \cdot R_A + \rho_B \cdot R_B}{(\rho_A + \rho_B)} \tag{24}$$

Thru an iterative process with equations 12.b to 24, the chemical kinetics residence time data derived in Figure 6 by MIT is data matched for oxygen and ethanol over an oxidizer to fuel ratio range of 1.1 to 1.3. By going through this procedure, we obtain the range of activation energy versus combustion temperature shown in Figure 8 for ethanol and oxygen.

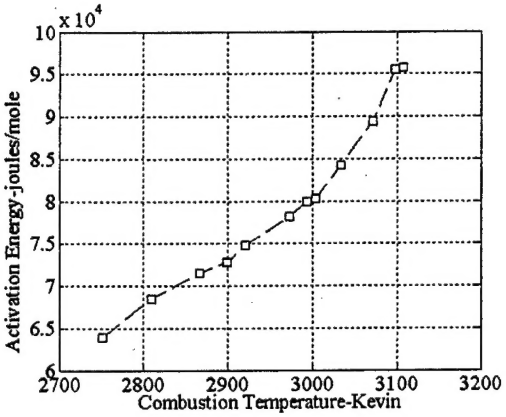

Figure-8. Activation Energy versus Combustion Temperature for Ethanol/Oxygen

II.C. Determining Minimum Chamber Size with MIT Combustion Analysis and Bimolecular Chemical Kinetics Model

The procedure to calculating the shortest combustion residence time is selecting a fuel-rich O/F ratio that minimizes the combustion temperature or activation energy in Figure 8, and which is still above the fuel-rich blow-out limit calculated by MIT in Figures 6 and 7. For this example, an O/F ratio of 1.2 was chosen just above the blow-out limit of 1.15 from the MIT data in Figure 6 and 7. This gives an activation energy , E_O, equal to 71,500 Joules/mole and will be the basis of a study to determine the minimum combustion residence time as the chamber characteristic time is reduced. This will be presented as the minimum chamber pressure required for complete combustion as engine characteristic length is reduced. This procedure starts with chamber residence time (Eq. 2) being set equal to or greater than the combustion residence time or

$$\tau_{res} \geq \tau_{comb} \tag{25}$$

From equation 2 and the definition for characteristic length[17], L_C, the chamber characteristic length can be defined as

$$L_C = \frac{V}{A_T} = \frac{\tau_{res} \cdot \dot{m}}{\rho_C \cdot A_T} \tag{26.a}$$

By substituting

$$\dot{m} = \rho_T \cdot A_T \cdot V_T = \rho_T \cdot A_T \cdot a_T$$

and τ_{comb} from equation 25, we finally get

$$L_C = \frac{\tau_{comb} \cdot \rho_T \cdot a_T}{\rho_C} \tag{26.b}$$

By assuming that the activation energy per mole, E_O, is independent of chamber pressure at the chosen O/F ratio of 1.2, then the combustion chamber residence time can be calculated as a function of chamber pressure with equation 12.b or

$$L_C = \frac{6}{N_{A_o} \cdot b \cdot K_{AB}} \cdot \frac{\rho_T \cdot a_T}{\rho_C} \tag{27}$$

From equation 27, the chamber characteristic length, L_C, for complete combustion is inversely proportional to the initial concentration of fuel for a constant value of K_{AB}, or inversely proportional to chamber pressure.

II.D. Determining Minimum Chamber Size utilizing the MIT Bipropellant Experimental Results and the Bimolecular Chemical Kinetics Model

MIT experimentally demonstrated a MEMS bipropellant engine[3] similar in size to the one shown in Figure 2. The experimental results were for gas to gas propellant mixing after injection into the MEMS combustion chamber with methane and oxygen as the propellants instead of ethanol and oxygen, the propellants in the analytical combustion study [9]. The procedure to matching the MIT experimental data involves determining the chamber pressure where exhaust velocity is maximized, determining the O/F ratio for these given conditions, and then determining the Arrhenius activation energy required to match the combustion residence time which is set equal to the chamber residence time of the MIT MEMS engine. The date matching procedure is similar to the data matching of the MIT bipropellant chemical kinetics analysis results shown in Figure 6, but is done differently depending upon the available experimental

data. To start the procedure, the chamber residence time (Eq. 2) for the MIT MEMS bipropellant engine is a fixed quantity independent of chamber pressure as discussed in the introduction and is equal to 0.1 msec. The combustion residence time is inversely proportional to chamber pressure represented by the initial fuel concentration, N_{A_o}, as determined by equation 12.b. By examining experimental data for characteristic exhaust velocity, c^*, as a function of chamber pressure, and determining the pressure where c^* reaches a maximum, the combustion residence time is then assumed to be equal to the chamber residence time at this set of test conditions. This assumption is valid because c^* is a slowly varying function of combustion temperature or

$$c^* = \sqrt{R \cdot T_c}\left(\frac{\gamma+1}{2\gamma}\right)^{\frac{\lambda+1}{2(\gamma-1)}} \qquad (28.a)$$

and is calculated experimentally with

$$c^* = \frac{P_c \cdot A_T}{\dot{m}} \qquad (28.b)$$

These characteristic velocity results are shown in Figure 9 for the MIT microrocket and indicates that c^* reaches a plateau around 7 atm.

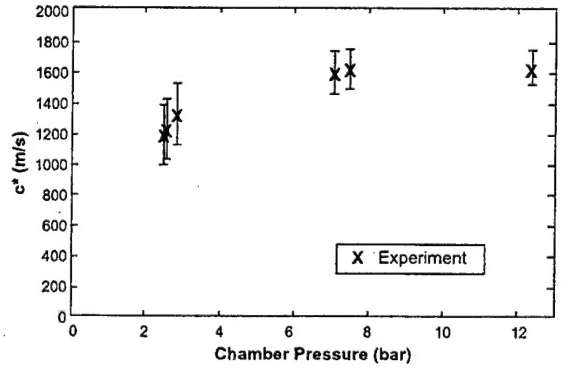

Figure-9. Experimental Measurement of Characteristic Velocity versus Chamber Pressure for MIT Microrocket (London,2001)

The next quantity required for data matching the experimental combustion results with the bimolecular kinetics model is the O/F ratio for the test in question. This is shown in Figure 10 and turns out to be approximately 2.6.

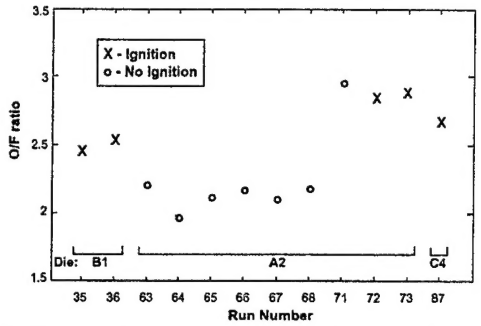

Figure-10. MIT Microrocket Ignition Results for Methane and Oxygen (London,2001)

Notice that the MIT microrocket has a narrow O/F operating range of 2.5 to 2.7, well below the stoichiometric value of 4.0 for oxygen and methane. This is just what you would expect from the chemical kinetics residence time modeling done by MIT[9] and shown in Figure 6. At the higher temperatures associated with stoichiometric combustion, the combustion residence time is much larger then the chamber residence time. In fact, during the MIT tests, the fuel-lean blow-out limit was reached at an O/F ratio of 3.0 as shown in Figure 10. In order to data match the MIT experimental combustion data with methane and oxygen, an Arrhenius activation energy of 91,500 Joules/mole was required. The final results for minimum chamber characteristic length versus chamber pressure for complete combustion from data matching both the MIT analytical chemical kinetics residence model[9], and the MIT experimental microrocket data[3], is shown in Figure 11.

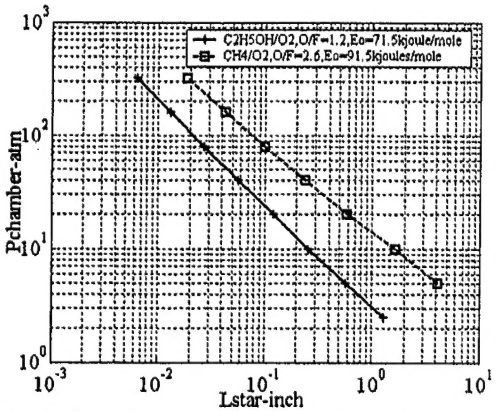

Figure-11. Minimum Chamber Characteristic Length versus Chamber Pressure for Complete Combustion

The resulting specific impulse from TEP analysis[12] was 345 seconds for methane and oxygen and 301 seconds for ethanol and oxygen at the chamber pressures required for complete combustion at these reduced engine characteristic lengths. The smaller the

combustion chamber, the higher the chamber pressure required to achieve complete, efficient combustion. These results only apply near the fuel-rich blow-out limit. At a stoichiometric O/F ratio, the chamber characteristic length would be orders of magnitude larger for complete combustion.

III. Application of High Thrust to Weight Ratio Bipropellant Thrust Vector Control to Reentry Vehicles Thru Micro-miniaturization

We have chosen the simplified reaction control system (RCS) analytical modeling in Reference 18 for evaluating microthruster TVC for two different weight class RVs. The large scale RV, shown in Figure 12, is a subscale wind tunnel model of a flapped RV configuration known as *MaRV* .

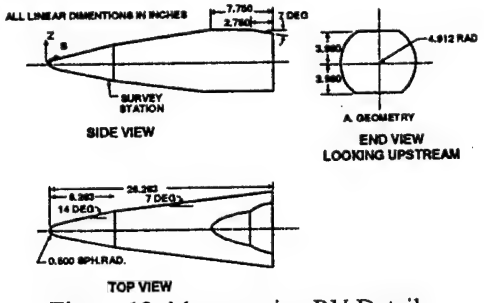

Figure-12. Maneuvering RV Details

To make this RV controllable with reaction control jets, the flaps are replaced with jet rows. For RCS thrusters of very small size, the jet rows would turn into thruster arrays which would cover the conic slice flat sections near the RV frustrum. The second RV is a much smaller RV known as a nano RV. A nano RV is shown in Figure 13 during full-scale ablation aerodynamics testing in the NASA Ames 20-mW arc jet[19]. Nano RVs are 1 to 2 orders of magnitude smaller than typical RVs. Typical pitch moment of inertias and lengths were used for an RV and nano RV in calculating RCS propellant consumption rate.

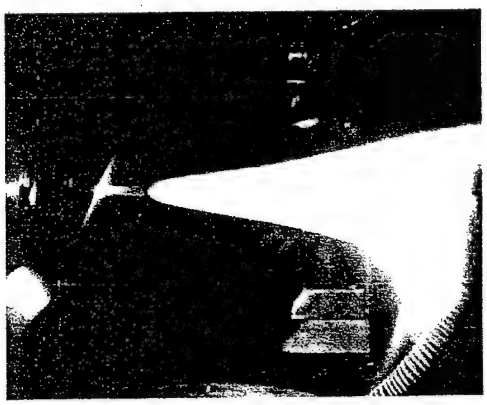

Figure-13. Nano Reentry Vehicle (Haldeman, 1986)

The RCS analytical model starts with determining the minimum RCS thrust requirements. These thrust levels are normally determined by the maximum allowable angular rates during certain RV functions such as star pointing, or GPS reception during exospheric coast after fourth-stage bus deployment prior to reentry or targeting maneuvers that require a given orientation or attitude. Because of the impossibility of imparting an infinitesimal small thrust amplitude to the RV, it is virtually impossible to obtain a given attitude with zero angular rate. As a result, the RV is kept at a given attitude within a dead-band region established by a limit-cycle amplitude shown in Figure 14.

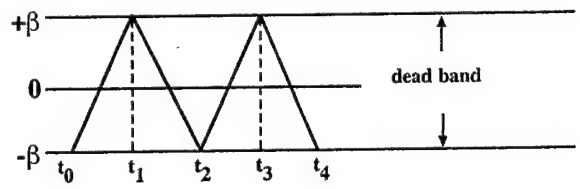

Figure-14. Reentry Vehicle Dead band Motion (Pohl, 1965)

To minimize RCS fuel consumption, the aerodynamic center of pressure is positioned at the center of gravity. The RV is not aerodynamically stabilized, but is stabilized with reaction control jets. The dead-band angular tolerance for attitude keeping is established by the attitude accuracy requirements.

To determine the RV RCS propellant consumption rate during limit-cycle operation, the procedures described in Reference 18 are used. If the limits of the dead band are $\pm\beta$, then the time history shown in Figure 14 results for the RV pitching motion. The propellant consumption per second of operation, W_p, for the limit-cycle pitching motion can be shown to be

$$W_p = \frac{(I^2)L}{4 \cdot J_x \cdot I_{sp} \cdot \beta} \tag{29}$$

where L is the reaction jet moment arm, I is the impulse bit (F.dt) provided by the reaction control jet, and J_x is the reentry vehicle polar moment of inertial. The attitude keeping propellant consumption rate, W_p,

is a strong, second-order function of the minimum impulse bit, I. The impulse bit wants to be as small as possible, especially for very small dead-band angular tolerances.

As an example, the attitude-keeping propellant consumption for a reentry vehicle reaction control system was calculated during exospheric coast after bus deployment and during reentry. As shown in Figure 15, by placing the center of pressure at the center of gravity, the RCS propellant consumption is minimized.

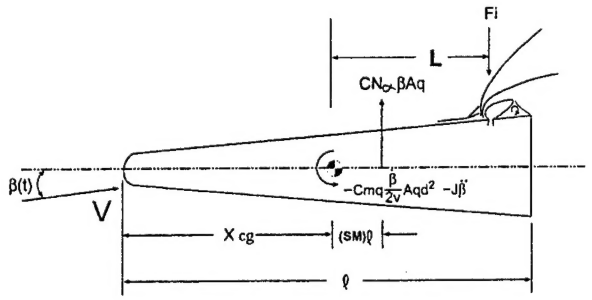

Figure-15. Reentry Vehicle Reaction Control System Forces and Moments

This results in the aerodynamic pitching moment, M_p, going to zero.

$$M_p = C_{n\alpha}.\beta \cdot A \cdot q \cdot sm \cdot l \rightarrow O \quad (30.a)$$

Also, the aerodynamic pitch damping, M_d, can also be neglected as follows

$$M_d = C_{mq} \cdot \frac{\dot{\beta} A}{2V} \cdot q \cdot d^2 \cong 0 \quad (30.b)$$

The pitch damping coefficient, C_{mq} can be shown to be small[20].

$$C_{mq} = C_{n\alpha}.2.(sm)^2 = 0 \quad (30.c)$$

Also, the induced angle of attack, $\frac{\dot{\beta} d}{V}$, during dead-band pitching motion is very small at reentry speeds. Essentially, the reentry vehicle has negligible aerodynamic damping, and aerodynamic pitching moment, or the propellant consumption rate for the RCS during both the exospheric and reentry portion of the RV trajectory can be calculated with equation 29.

Another interesting feature about reaction control jets is their interaction with surrounding air flow during reentry as illustrated in Figure 15. This control jet interaction increases the effectiveness of the control jet[21]. This increased effectiveness is usually referred to as the thrust amplification factor and is defined as

$$K_f = \frac{F_i + Thrust}{Thrust} \quad (31)$$

Some data for k_f as a function of temperature and molecular weight of exhaust products is shown in Figure 16.

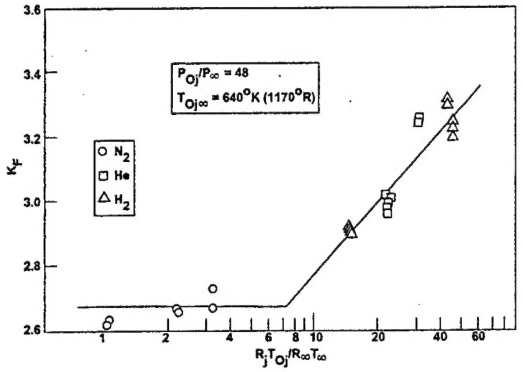

Figure-16. Dependence of the Jet Thrust Amplification Factor, K_f, on Temperature and Molecular Weight

By assuming a 60-percent increase in reaction jet thrust (k_f equal to 2.6), then the effective I_{sp} will be about 60-percent higher due to jet interactions with the freestream during reentry.

An estimate of the minimum impulse bit, I, has to be made in order to calculate the limit-cycle fuel consumption rate, W_p. By photographically sub-scaling the MIT MEMS bipropellant engine (Figure 2), and utilizing the minimum chamber pressure for complete combustion versus chamber characteristic length results in Figure 11, an estimate of the minimum obtainable thrust as a function of engine characteristic length can be made. These microthruster results are shown in Figure 17 for methane/oxygen and enthanol/oxygen propellants.

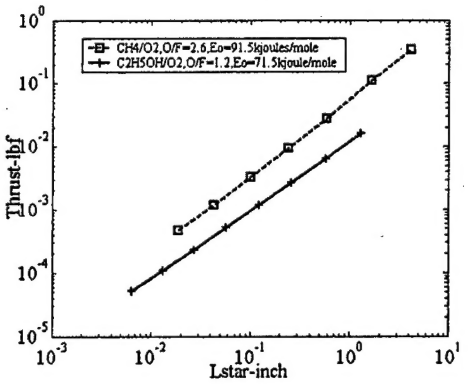

Figure-17. Minimum Obtainable Microjet Thrust versus Chamber Characteristic Length

It is interesting to note, that because the minimum chamber pressure for complete combustion versus chamber characteristic length is utilized in the calculation, the minimum obtainable thrust versus chamber characteristic length results from the calculation. I, the minimum obtainable impulse bit, is calculated with the minimum obtainable thrust as follows.

$$I = \int_0^{\Delta T} F dt \tag{32}$$

An estimate of 2 milliseconds for valve opening time, ΔT, was made[22]. Valve leakage rates should not be a major concern for RVs because the operational mission is usually 20 minutes or less from the fourth-stage bus dispense to impact. Satellite station keeping with much longer operational missions lasting months to years, would have to address valve leakage issues.

The final quantity required before calculating the dead-band limit-cycle propellant consumption rate, is the dead-band angular target pointing tolerance, β, in Figure 14. Due to RV ablation shape change aero uncertainties, this dead-band target pointing tolerance, $\pm\beta$, was set to $\pm$ 0.1 degree [23,24].

Finally, the mission impulse requirements for the dead-band limit-cycle is calculated as follows

$$I_T = \sum W_{P_i} . \Delta T_i . I_{sp_i} \tag{33}$$

I_{SP_i} is varied for reentry with jet interaction argumentation, or for vacuum thrust performance during the exospheric dispense from the fourth-stage RV bus. The trajectory time, ΔT, is for a typical exospheric suborbital ballistic trajectory, and a typical atmospheric reentry to impact. The final mission impulse energy requirements are shown in Figure 18 for the dead-band pointing limit-cycle as a function of microthrust engine characteristic length.

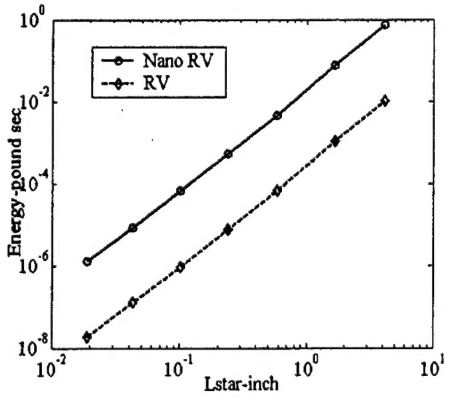

Figure-18. RV RCS Mission Impulse Requirements for Dead-Band Targeting Motion

The dead-band pointing tolerance energy consumption is quite small, and in reality, any deviation from the target flight path would require significantly more RCS total impulse then shown due to ablation shape change, and changes in aerodynamic center of pressure during reentry. What this mission impulse requirements analysis in Figure 18 does show is for smaller values of the minimum impulse bit, I, the smaller the mission impulse requirements to maintain a given dead-band pointing tolerance. Also, the nano RV has higher mission impulse requirements than the RV for a given thruster characteristic length because the microthruster is initially oversized. Basically, the smaller the RV, the smaller the minimum impulse bit required to maintain a given pointing angular tolerance. For tactical warhead RV applications, the RV has to have central error probable (CEP) of 15 feet to be effective[24]. Having RCS thrusters with a very small minimum impulse bit goes a long way to achieving this accuracy requirements.

IV. Conclusions

Small-scale flight vehicles make outstanding missile payloads such as a MEMS satellite, or nano RV where the enhanced drag characteristics of a reduced mass vehicle is an advantage during reentry. Using MEMS technology to develop a reduced scale launch vehicle is counter productive because of the reduced payload mass fraction resulting from increased

aerodynamic losses at reduced scales. The enhanced drag characteristic of nano RVs during reentry is beneficial, because they will decelerate below the plasma shielding velocity more quickly allowing more time for target acquisition and seeking. This also implies that in order to take advantage of the high T/W ratio enhancement of microthruster engines, they should be clustered into larger arrays propelling larger vehicles. In this way, the reduction in propulsive engine weight in relation to the overall vehicle weight would be realized without a corresponding loss in payload mass fraction due to the enhanced effects of air drag on reduced-scale vehicles.

There are a few other caveats associated with using the MEMS combustion results described in the theoretical section. First, MIT demonstrated their bipropellant microthruster with nonhypergolic propellants. For a TVC microthruster application where a small minimum impulse bit is desired, hypergolic or catalyzed monopropellants would be the preferred propellant to facilitate the intermittent duty ignition requirement for TVC. Hypergolic ignition followed by steady-state combustion has not been demonstrated at MEMS microthruster scales as of this time. The hypergolic or spontaneous ignition delay would have to be accounted for in the combustion residence time analysis discussed previously in follow-up analysis[25]. This would involve spark or spontaneous hypergolic ignition being investigated at elevated chamber pressures in order to achieve steady-state combustion at smaller and smaller engine scales. The important thing is that MIT has demonstrated rocket bipropellant combustion at reduced engine scales. The solution to the spontaneous or spark ignition problem at reduced scales is fundamentally similar in nature to the reduced-scale combustion problem. Another caveat is that MIT demonstrated reduced-scale combustion with gaseous bipropellant injection mixing prior to combustion. Gaseous bipropellant injection may be also required for hypergolic ignition to be successful. This brings up another important area for investigation at reduced MEMS engine scales, the mixing time scales associated with bipropellant liquid to liquid injection prior to combustion. Droplet evaporation times should be investigated at reduced engine scales as follow-up combustion analysis.

Thrust to weight ratio may be enhanced dramatically at reduced bipropellant engine characteristic lengths, but the achievement of a small minimum impulse bit as a result of reduced engine characteristic length is not to be ignored in reducing TVC fuel consumption rate as shown in Equation 29. The TVC propellant consumption rate, $\dot{W}_P$, was dramatically reduced for smaller engine characteristic lengths during RV RCS attitude keeping dead-band limit-cycle analysis. Another area for future investigation would be regenerative cooling for intermittent duty microthrusters in order to maintain high I_{SP} operation.

As a final note, the challenges ahead at achieving the bipropellant TVC microthrusters described in this paper are formidable. As Prof. Robert C. Haddon said during a public gathering introducing the new UC Riverside Center for Nanoscale Science and Engineering[26], "To make contributions to the field of nanotechnology, you have to be an inch deep and a mile wide". MEMS and nanotechnology involve so many disciplines, that the engineer has to have a very open mind and to think outside of the box to make contributions to microthruster propulsion applications. MEMS and nanotechnology engineering represent new, and challenging paradigms on how to address traditional propulsion engineering[27].

V. Acknowledgements

The author would like to acknowledge the help of the MIT Gas Turbine Lab, in particular, Prof. Alan Esptein, in providing critical MEMS engine design and performance characteristics without which this technical effort would have been very difficult to complete. Although the views of this author may differ from the principle technical contributors in how MEMS bipropellant microthrusters should be applied, it is nevertheless agreed that the MIT Gas Turbine Lab design and demonstration of a MEMS bipropellant microthruster was a major breakthrough in the understanding of rocket engine combustion phenomena at reduced residence times and engine scales.

VI. Nomenclature

A	Molar concentration of fuel	$\left[moles/m^3\right]$
A_T	Throat area	$\left[ft^2\right]$
a_T	Throat sonic velocity	$\left[ft/\sec\right]$
B	Molar concentration of oxidizer	$\left[moles/m^3\right]$
b	Oxidizer stoichiometric coefficient	$[-]$
C_f	Thrust coefficient	$[-]$

12. TEP Version 1.5, SEA Software, Inc., 1802 N. Carson Street, Suite 200, Carson City, NV 89701.

13. Toong, "Chemical Kinetics – Chapter 4", Combustion Course Notes for MIT Course 2.282, pp. 4-2 to 4-14.

14. Boyce, W.E., Di Prima, R.C., "Elementary Differential Equation", John Wiley and Sons, Inc., Second Edition, Copyright 1969, pp.59-60, p. A-6.

15. Lewis, B., Von Elbe, G., "Combustion, Flames, and Explosion of Gases", Academic Press, Inc, Copyright 1987, pp.10-13, pp.25-38.

16. Lee, J.F., Sears, F.W., "Thermodynamics-An Introductory Text for Engineering Students", Addison-Wesley Publishing Company, Inc., Copyright 1963, Second Edition , pp. 354-371, p. 28.

17. Sutton, George P., "Rocket Propulsion Elements", 3rd Edition, Copyright 1963, John Wiley & Sons, Inc., p. 233.

18. Pohl, H.A., "Manned Spacecraft Engineering, Design, and Operations", Edited by M.A. Faget, N.F. Smith, and P.E. Purser, (Fairchild Publications, New York, 1965), Chapt. 27.

19. Haldeman, C.W., Figueiredo, W.A., Weinburg, A.D., "MIT/Ames 20-MW Arc Jet Force Test Plan-Measurements of Rotating Conical Reentry Vehicle Ablation Aerodynamics", MIT Lincoln Laboratory, October 1986.

20. Etkin, B., "Dynamics of Flight, Stability and Control", Copyright 1959, John Wiley & Sons, Inc, p. 155.

21. "Proposal to Analyze Reaction Control-Induced Aerodynamic Interference for Space Shuttle", MDC G2703P, McDonnell Douglas Astronautics Company, December 1977.

22. Bryant, K., Knight, C., and Hurtz, R., "Planetary Lander Vehicles Utilizing LEAP Technology", 30th AIAA/ASME/SAE/ASEE Joint Propulsion Conference, AIAA Paper No. 94-2748, June 27-29, 1994.

23. Cassel, L.A., Traci, R.M., McMillen, L.D., "Aerodynamic Uncertainties Modeling for Advanced Terminal Defense Interceptors", Ballistic Missile Defense Advanced Technology Center, Missile Directorate-BMDATC-M, Contract Number DASG60-76-C-0042, 7 February 1977.

24. Cassel, L.A., Siemons, E.H., " Modeling Aerodynamics Uncertainties Error Sources in Simulation of Hypersonic Missile Performance", Ballistic Missile Defense Advanced Technology Center, BMDATC/M, P.O. Box 1500, Huntsville, Ala. 35807, Contract No. DASG60-77-C-0149, 2 January 1979.

25. Spalding, D. Brian, "Combustion and Mass Transfer", Spontaneous Ignition, Pergamon Press Ltd., ISBN 0-08-022106-8, pp. 272-293.

26. "Nanotechnology-UC Riverside Leadership, A Conversation with Robert C. Haddon", University of California, Riverside, Fiat Lux, Winter 2002, Volume XII, Number 4, Fiatlux.edu, pp.22-23.

27.Wilson J.R., "Major New Thrust for MEMS Engines", Aerospace American, February 2003, pp.34-38.